Observation of deep level defects within the waveguide of red-emitting high-power diode lasers

Claus Ropers, Tran Quoc Tien, Christoph Lienau, and Jens W. Tomm[a)]
Max-Born-Institut, Max-Born-Strasse 2 A, 12489 Berlin, Germany

Peter Brick, Norbert Linder, Bernd Mayer, Martin Müller,
Sönke Tautz, and Wolfgang Schmid
Osram Opto Semiconductors GmbH, Leibnizstrasse 4, 93055 Regensburg, Germany

(Received 21 October 2005; accepted 14 February 2006; published online 30 March 2006)

The waveguides of 650 nm emitting high-power laser diodes are analyzed regarding the presence of deep level defects by photoelectrical techniques, namely, photocurrent spectroscopy, laser beam induced current, and near-field optical beam induced current (NOBIC). Deep level configurations in pristine devices and the kinetics of defect creation during device operation are monitored and discussed. The localization of the defects within the epitaxial layer sequence is done by NOBIC. We show that light, which is confined within the laser waveguide, interacts with the deep level defects detected. This demonstrates that the presence of deep level defects directly affects the device properties. © *2006 American Institute of Physics*. [DOI: 10.1063/1.2190815]

Since the invention of red-emitting cw InGaAlP laser diodes about 20 years ago,[1,2] these devices found a number of important widespread applications such as in barcode readers, color printers, and for optical disks. For more powerful devices with emission powers exceeding 100 mW, there are a number of additional options. Among others, these lasers can serve as direct pump sources for CrLiSAF femtosecond lasers and provide one basic color in laser displays. Furthermore, medical applications such as photodynamic therapy, photostimulated wound or burn healing, and surgery represent additional fields. This second group of applications requires both a high output power in the 0.1–1 W range and a sufficient long-term reliability of some thousand hours. In contrast to this demand, red-emitting high-power devices still exhibit inferior performance and reliability figures compared to the established InAlGaAs high-power laser diodes emitting in the near infrared. Overcoming of these drawbacks is considered essential in order to push novel applications.

The goal of this study is to get insight into the impact of deep level defects[3] on the degradation of red-emitting high-power laser diodes. Milestones are the evidence of such defects in pristine devices as well as the demonstration of a correlation between power degradation of devices and increased deep level concentration. In this Letter, we focus on the localization of the defects within the epitaxial layer sequence. These results demonstrate that light, which is confined within the laser waveguide, indeed couples strongly to the monitored deep level defects revealing the link between the presence of deep levels and output properties for this class of devices.

The 650 nm emitting high-power diode laser devices are based on metal-organic vapor-place epitaxy (MOVPE)-grown InGaAlP structures. One single 5 nm thick InGaP quantum well (QW) is embedded into an InGaAlP waveguide; see Fig. 1(a). *P*- and *n*-side dopings are implemented by Mg and Te, respectively. The layer sequence is finished by a 0.4 μm thick highly doped *p*-GaAs contact layer. From these structures broad-area single-emitter chips are prepared. The cavity length is 1200 μm, whereas the emitter stripe width is 100 μm; see Fig. 1(b). By mounting these chips *p* side down onto C mounts, the threshold current is found to be at about 450 mA with a differential efficiency of 0.8 W/A. As a consequence 500 mW are easily reached for operation currents of about 1.1 A. Analyzing these devices in aging tests, no significant performance degradation occurs during 1000 h of operation. Here we present data from devices originating from four different epitaxial test batches.

Analysis of the deep level configuration within the waveguide of the devices is made by three complementary photoelectrical techniques, namely, photocurrent spectroscopy (PCS), laser beam induced current (LBIC), and near-field optical beam induced current (NOBIC). Such a concerted approach to red-emitting devices is reported here—to the best of our knowledge—for the first time. PCS allows for monitoring absorption spectra of the laser waveguide.[4,5] The achievement of signal-to-noise ratios of $>10^6$, see Fig. 2(a), allows for analyzing even the weak absorption shoulders caused by (de)ionization of deep level defects [defect-to-

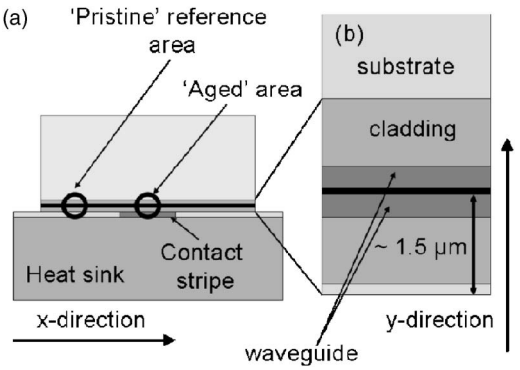

FIG. 1. (a) Schematic diagram of the front view of a red-emitting high-power laser diode. The areas, where the NOBIC experiments are performed, are marked by full circles. (b) Schematic of the epitaxial layer sequence of the laser structure.

[a)]Author to whom correspondence should be addressed; electronic mail: tomm@mbi-berlin.de

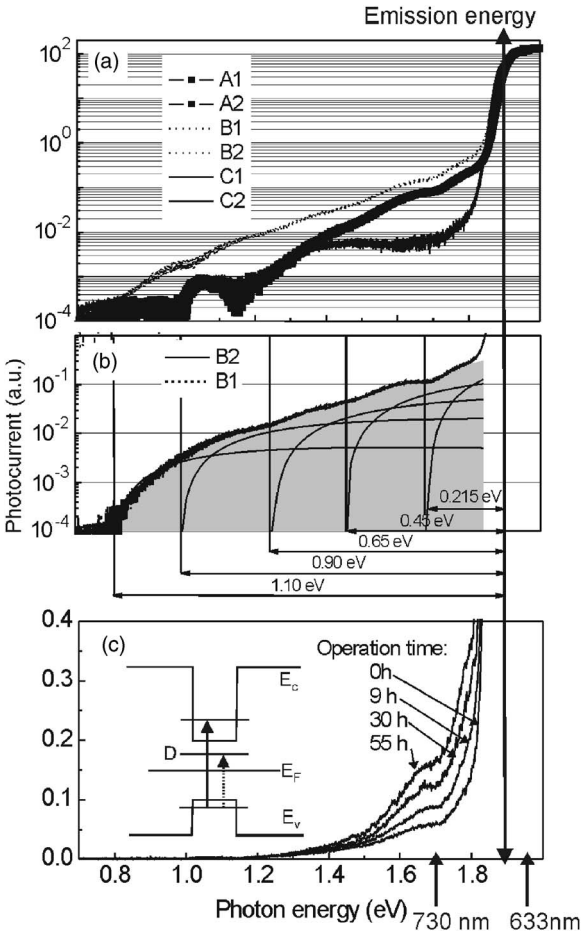

FIG. 2. (a) Photocurrent spectra from six red-emitting high-power diode lasers being prepared from three epitaxial test batches (A, B, and C). The spectra from the individual devices (in each batch denoted as 1 and 2) are almost identical, and therefore hard to distinguish in this display. (b) Fit of the spectra from devices B1 and B2 by five defect level-to-band transitions. The "level depth" corresponding to the particular optical transition is indicated. The gray area marks the sum of the five contributions matching the experimental data. (c) Photocurrent spectra from the pristine device D1 and subsequent spectra monitored after 9, 30, and 55 h of regular operation at 0.9 A cw. The arrows mark those wavelengths that are employed for the experiments on the defect localization. The inset shows a simplified level scheme including valence (E_v) and conduction (E_c) bands, the Fermi level (E_F), and a defect level (D). The arrows indicate optical interband (full arrow, 633 nm) and defect excitation (ionization, dotted line, 730 nm) resulting in respective photocurrents.

(mini-)band transitions]. The spatial resolution of this technique, however, is rather poor (excitation spot $\varnothing = 400$ μm in the present experiments). The LBIC technique relies on monochromatic (laser) excitation and provides scans of "photocurrent versus position," e.g., along devices.[6] The setup used in this study has a spatial resolution of about 10 μm (width of the excitation light line formed by a cylindrical lens) when scanning in one dimension, e.g., along the x axis perpendicular to the growth direction; see Fig. 1(a). NOBIC (Ref. 7) is considered an extension of LBIC with increased spatial resolution of about 150 nm, when scanning, e.g., with 730 or 633 nm excitation light. The subwavelength spatial resolution is achieved by replacing the narrow excitation light stripe of the LBIC measurement by the aperture of a fiber tip of a near-field scanning optical microscope. The use of Y couplers for feeding light from the different laser sources [HeNe (633 nm) and Ti: sapphire (730 nm)] into the fiber tip allows to carefully control the amount of light coupled into the fiber tip (error less than 5%). Our NOBIC experiments include the simultaneous measurement of photocurrent (signal, phase) and topographic maps of an area of 2.15×2.15 μm^2. In the following discussion we use scans across the laser facet along the growth direction, here called the y direction; see Fig. 1(b). For all these techniques, photons of an energy smaller than the fundamental QW transition energy couple to defects within the waveguide of the device. Excited carriers are subsequently freed by thermionic emission and separated by the built-in voltage of the unbiased *pn* junction of the device. Moving carriers cause the photocurrent, which is measured via the contacts of the packaged device. The process of photocurrent generation by below-band-gap excitation of defects takes place in the same way known from so-called extrinsic infrared detectors (e.g., Ge:Au). The only difference is that the external voltage applied to the latter is replaced by the built-in voltage of the unbiased *pn* junction in the present case. The inset in Fig. 2(c) gives a level scheme, which illustrates the QW transitions (full arrow) and one single deep-level-related transition (dotted arrow). The successful combination of all three complementary techniques relies on careful shielding, low-noise preamplification, and lock-in detection.

Starting the spectroscopic analysis with PCS, Fig. 2(a) shows typical spectra from six pristine red-emitting devices belonging to three different epitaxial batches (A, B, and C). At about 1.9 eV ($\sim$650 nm, see arrow across all parts of Fig. 2) a pronounced absorption edge due to the ground-state transition in the QW is observed. At lower energies, shoulders caused by deep level defects are visible. Since the spectra from devices of the same epitaxial run, e.g., A1 and A2 show almost identical spectra, we consider these low-energy shoulders as being "batch specific." In Fig. 2(b) we present a fit of the shoulders found in the PCS spectra of devices B1 and B2 to five transitions via deep levels with depths of 1.10, 0.90, 0.65, 0.45, and 0.215 eV. The gray area illustrates the sum of all these contributions, which are calculated according to an early model introduced by Lucovsky.[8]

Batch D, in general, showed an inferior long-term reliability (degradation rate $\sim 10^{-3}$ h^{-1}) compared to previously discussed charges A–C. It shows more pronounced deep level contributions but with the same energetic depths as observed for the regular charges. This made batch D a promising candidate for aging experiments. Figure 2(c) displays PCS spectra from device D1 monitored at various operation times during burn-in (note the linear ordinate). A substantial increase of the 0.45 and 0.215 eV deep level contributions, is observed for the device operation times of up to 55 h. In addition, we found that during this time the emission power dropped by 11%, establishing a correlation between defect concentration and device degradation.

Figures 3 present our results on the spatial localization of the deep level defects observed in device D1. In Fig. 3(a), LBIC data, obtained for resonant defect level excitation, are reported. Obviously, in the active region, i.e., underneath the metallized emitter stripe, a substantial operation-induced increase of the deep-level-related photocurrent is observed. Thus, there is a clear correlation between the stripe region, which experienced the load during operation, and the creation of operation-induced deep level defects. Following this "rough" lateral localization along the x direction, Figs. 3(b) and 3(c) provide now the vertical localization by NOBIC on a nanometer scale. This is essential for our line of argument,

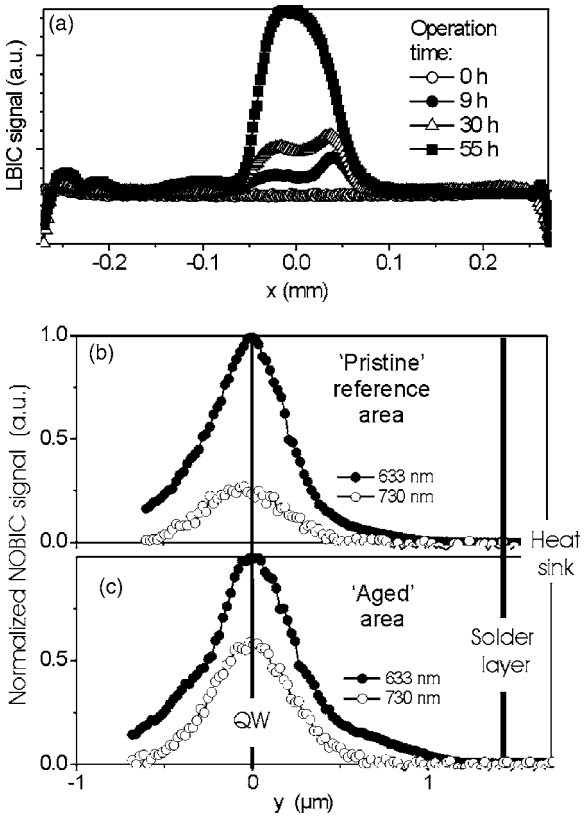

FIG. 3. (a) LBIC scans taken at 730 nm along the front facet of device D1 monitored after 9, 30, and 55 h of regular operation at 0.9 A cw. A substantial increase of the defect-related photocurrent during device operation is observed. [(b) and (c)] Near-field optical beam induced current scans parallel to the growth direction across the active region of the device. The full circles represent data obtained at an excitation wavelength of 633 nm, while the open circles denote data obtained for 730 nm excitation. The scan was extended across the solder layer to the heat sink in order to ensure that even the highly doped GaAs contact layer is completely included.

because, e.g., also the 0.4 μm thick highly doped p-GaAs contact layer is another likely candidate for generation or accumulation of deep level defects during high-power operation. Since this contact layer is separated from the QW by only 1.1 μm, see Fig. 1(b), LBIC data would not allow for an unambiguous assignment. For this particular NOBIC experiment, we use device D1 after 55 h of operation in order to avoid measurements (and alignment) before and after device aging. As "pristine" reference area serves a region outside the emitter stripe, which has not been affected by the high current density during the 55 h of operation; see circles in Fig. 1(a). NOBIC scans are taken at excitation wavelengths of 633 and 730 nm [see arrows in Fig. 2(c)], respectively. The first one provides interband excitation of the QW, whereas 730 nm matches the maximum of the absorption band of the defect band, which starts at 450 meV below the QW band edge. Comparing the normalized Figs. 3(b) and 3(c), the most striking feature is a 2.3-fold increase in the deep level defect contribution to the photocurrent in the "aged area" below the emitter stripes with respect to that in the pristine reference area. This type of experiment has been repeated four times at different locations within and outside the contact stripe. In all cases the "aged" area reproducibly exhibited a two to three times increase in the defect-related photocurrent (730 nm) compared to the interband one (633 nm), which serves here as the reference.

Even though a detailed discussion of the microscopic nature of the detected deep level defects is far beyond the scope of this report, we can draw some conclusions about their microscopic nature. Since we do not observe any dark-line or dark-spot defects within pristine devices, we assign the observed defects to point defects, probably caused by native point defects (e.g., vacancies or interstitials) or foreign impurity atoms. Figure 2(a) shows clearly that the ratio of the different contributions changes depending on the particular epitaxial test batch. Thus it is likely that a number of physically different types of defects contribute to the creation of the five absorption shoulders. The defect contributions with depths, of 1.1 and 0.9 eV are considered to be created by midgap states, which probably also act as recombination centers for processes of the Shockley-Reed-Hall type. Our experiments on the localization of the deep level defects still leave the localization along the laser axis (z direction) open. Therefore we have to clarify whether the deep level defects are concentrated beyond the front facet or distributed along the whole cavity. Another important issue is the search after a correlation between the deep level configuration within a particular epitaxial batch and the long-term reliability of devices prepared from it. Work on these key topics is underway.

In summary, we have analyzed waveguides of red-emitting high-power diode lasers regarding the presence of deep level defects. Deep level configurations in pristine devices are analyzed and the kinetics of defect creation during device operation is monitored. For the pristine devices, a fit of the absorption bands monitored by photocurrent measurements reveals level depths of 1.10, 0.90, 0.65, 0.45, and 0.215 eV. For one device batch we showed the concentration of the 0.45 and 0.215 eV deep defect levels to grow within 55 h of device operation. In addition, we provide a clear localization of the defects within the epitaxial layer sequence by using LBIC and NOBIC. We show that light, which is confined within the laser waveguide, interacts with the deep level defects detected. As a consequence, these defects, if present in higher densities, can affect device properties in a direct way.

This study was funded by the European Union within the project WWW.BRIGHT.EU, Contract No. 511 722.

[1]M. Ikeda, Y. Mori, H. Sato, K. Kaneko, and N. Watanabe, Appl. Phys. Lett. **47**, 1027 (1985).
[2]K. Kobayashi, S. Kawata, A. Gomyo, I. Hino, and T. Suzuki, Electron. Lett. **21**, 931 (1985).
[3]We use the term "deep level defects" to denote foreign and native defects, which are not described by the effective mass approximation, i.e., not "hydrogenlike" defects.
[4]C. H. Henry, P. M. Petroff, R. A. Logan, and F. R. Merritt, J. Appl. Phys. **50**, 3721 (1979).
[5]J. W. Tomm, A. Bärwolff, A. Jaeger, T. Elsaesser, J. Bollmann, W. T. Masselink, A. Gerhard, and J. Donecker, J. Appl. Phys. **84**, 1325 (1998).
[6]C. J. R. Sheppard, Scanning Microsc. **3**, 15 (1989).
[7]A. Richter, J. W. Tomm, Ch. Lienau, and J. Luft, Appl. Phys. Lett. **69**, 3981 (1996).
[8]G. Lucovsky, Solid State Commun. **3**, 299 (1965).